Progress in Biomaterials (2021) 10:281–297
https://doi.org/10.1007/s40204-021-00172-5

ORIGINAL RESEARCH

Chitosan-coated pore wall polycaprolactone three-dimensional porous scaffolds fabricated by porogen leaching method for bone tissue engineering: a comparative study on blending technique to fabricate scaffolds

Deepak Poddar[1] · Misba Majood[2] · Ankita Singh[1] · Sujata Mohanty[2] · Purnima Jain[1]

Received: 30 July 2021 / Accepted: 6 November 2021 / Published online: 25 November 2021

Abstract

One of the significant challenges in the fabrication of scaffolds for tissue engineering lies in the direct interaction of bioactive agents with cells in the scaffolds matrix, which curbs the effectiveness of bioactive agents resulting in diminished cell recognition and attachment ability of the scaffolds. Here, three-dimensional porous scaffolds were fabricated using polycaprolactone (PCL) and chitosan, by two approaches, i.e., blending and surface coating to compare their overall effectiveness. Blended scaffolds (Chi-PCL) were compared with the scaffolds fabricated using surface coating technique, where chitosan was coated on the pore wall of PCL scaffolds (C-PCL). The C-PCL exhibited a collective improvement in bioactivities of the stem cell on the scaffold, because of the cell compatible environment provided by the presence of chitosan over the scaffolds interface. The C-PCL showed the enhanced cell attachment and proliferation behavior of the scaffolds along with two-fold increase in hemolysis compatibility compared to Chi-PCL. Furthermore, the compression strength in C-PCL increased by 24.52% and 8.62% increase in total percentage porosity compared to Chi-PCL was attained. Along with this, all the bone markers showed significant upregulation in C-PCL scaffolds, which supported the surface coating technique over the conventional methods, even though the pore size of C-PCL was compromised by 19.98% compared with Chi-PCL.

Keywords Bone tissue engineering · Comparison · PCL-chitosan scaffolds · Porogen leaching · Surface coating method · 3-D scaffolds

Introduction

Various polymers, ceramics, and their combinations have been explored for desired properties and needs of various biomedical application. The primary prerequisite is to obtain the appropriate mechanical strength, tenable biodegradability, incorporation of growth factors, and many more as an alternative for bone tissues in biomedical application (Dhandayuthapani et al. 2011; Shkarina et al. 2018). In the recent past, researchers have shown keen interest in using synthetic polymers like polycaprolactone (PCL), polyvinyl alcohol (PVA), polylactic acid (PLA), and poly lactic-*co*-glycolic acid (PLGA) for the fabrication of porous scaffolds for tissue engineering application (Wu et al. 2017; Baptista and Guedes 2021). These polymers are FDA approved and are successfully used as orthopedic implants where these polymers serve appropriate mechanical strength, structural integrity, and controlled

✉ Sujata Mohanty
drmohantysujata@gmail.com

✉ Purnima Jain
prnm_j@yahoo.co.in

Deepak Poddar
poddardeepakpoddar@gmail.com

Misba Majood
misbatps@gmail.com

Ankita Singh
ankitachem17@gmail.com

[1] Department of Chemistry, Netaji Subhas Institute of Technology, University of Delhi, Dwarka Sector 3, New Delhi 110078, India

[2] Stem Cell Facility, DBT-Centre of Excellence for Stem Cell Research, All India Institute of Medical Sciences, New Delhi 110029, India

biodegradability (Wei et al. 2006; Kim and Kim 2014; Saito et al. 2015). However, they lack the properties like cell proliferation, osteo-conductivity, and biocompatibility, which restricts their use in tissue engineering (Poddar et al. 2021).

Though the use of natural-based polymers, such as chitosan, collagen, cellulose, and few bio-ceramic materials, such as hydroxyapatite and bioactive glass, is considered to be as bioactive agents and are proven to be preferred solutions for the limitation as mentioned above, i.e., these materials provide excellent biocompatibility, better cell recognition, controlled biodegradability, non-toxicity, and other chemical properties which help in better cell growth due to the presence of legends, such as amino and hydroxyl functional groups, that are confessed by cell surface receptors (Kane and Roeder 2012; Xia et al. 2017; Xing et al. 2019; Farzinfar and Paydayesh 2019; Boido et al. 2019; Distler et al. 2020; Abdel-Mohsen et al. 2020). Furthermore, natural polymers and ceramics tend to degrade into tiny fragments of amino molecules that are non-toxic and are readily absorbed in the human body after degradation (Zarrintaj et al. 2018). However, a natural polymer shows insufficient mechanical strength due to its brittle nature, limiting its clinical utility in load-bearing applications (Depan et al. 2011).

Fabrication methods and scaffold architecture play a significant role in material selection for their performance, such as mechanical strength and cell attachment ability. Several methods have been adopted to fabricate scaffolds, such as dip coating method (Panas-Perez et al. 2013), nesting (Guoping Chen et al. 2000), blending (Ghorbani et al. 2016), templating of natural polymers (Gao et al. 2016), or ceramic on synthetic polymers (Sari et al. 2021), which considerably improves biocompatibility, cell recognition and attachment of the scaffolds (Naahidi et al. 2017; Saroia et al. 2018). Among these methods, blending is one of the most explored, easy, and practical approach for the fabrication. The process involves blending of above two classes of polymers with the tailored properties to attain the required set of derived properties from both polymers, such as biocompatibility from the side of natural polymers and mechanical strength, controlled biodegradability and structural integrity from the group of synthetic polymers (Rodrigues et al. 2021; Nahanmoghadam et al. 2021). The compatibility between the polymers is one of the main obstacles faced in the fabrication process (Zhao et al. 2018). Additional limitations include compromising the strength of synthetic polymer due to natural part and limited exposure of the natural polymer on the surface of the scaffolds. The blending of the bioactive agents leads to its masking by a polymeric matrix, limiting the exposure of the bioactive agents with the cells and diminishing the osteo-conductivity properties of polymeric matrix and cell growth ability (Li et al. 2012). Therefore, to improve the cell recognition behavior, the direct interaction of the cell with the growth factor by surface coating methods is considered a practical approach (Li et al. 2012).

Furthermore, the polymer selection was made based on the previous study (Jain et al. 2015)**.** PCL was selected as a matrix for the scaffolds due to its slow, controlled degradation, suitable compressive strength (Miszuk et al. 2021; Siddiqui et al. 2021),modulus, common solubility with chitosan, and enhanced bone growth and mineral deposition ability (Nair and Laurencin 2007; Cipitria et al. 2011). Chitosan was selected based on its ability to promote tissue growth, high osteo-conductivity, wettability, and differentiation during wound healing and cationic studies (Raftery et al. 2015).

In this study, one of the most commonly adopted methods for the fabrication of the scaffolds, such as blending the two sets of polymers (natural and synthetic polymers) to extract the synergic properties, is compared with the unconventional approach of fabrication in which chitosan was coated on the surface of pore wall of PCL scaffolds. The presence of chitosan as a bioactive coated on the surface of PCL will help provide improved biocompatibility, cell interaction, cellular uptake, and many more, as the presence of amino and hydroxyl groups in the backbone of chitosan will augment the wettability and compatibility to the system. The coating method tends to surpass the limitation of blended scaffold compatibility and provide control over surface exposure and negotiate the compromise in properties of both polymers. The comparison was made based on their mechanical, morphological, and biological aspects for the three-dimensional porous polymer scaffolds fabricated by blending and coating methods.

Material, methods, and characterization

Materials

Polycaprolactone refined power (M_n 50 kDa) was purchased by Sigma Aldrich India, Chitosan (M_w 170 kDa), paraffin wax ($T_m = 53–56$ °C), 1% Triton X-100, dexamethasone, β-glycerolphosphate, ascorbic acid 2 phosphate, 10% MTS purchased from sigma. TriReagent, cDNA was purchased form Thermo Scientific. Other solvents and chemicals have been purchased from CDH Chemical and further used without any purifications.

Methods

Fabrication of paraffin microsphere (PMS)

The paraffin microsphere was fabricated using the oil–water suspension method. Gelatin 0.5% (w/v) was dissolved in distilled water (DI) at 80 °C till the clear solution was achieved, followed by the addition of paraffin pellets 5% (w/v) in the

above solution. The above suspension was stirred at 80 °C at 1250 rpm for homogenization, and subsequently, the suspension was quenched using ice-cold water. Further, the solution was filtered using the vacuum filtration assembly and washed with water and acetone for the removal of gelatin.

Fabrication of surface-coated scaffolds

For the preparation of C-PCL scaffolds, a series of steps have been performed, (step 1) PMS 10% (w/v) was suspended into the 3% (w/v) chitosan solution (2% (v/v) acetic acid), followed by the sponge preparation using modified mold setup. Briefly, the above suspension was placed in a 10 mL plastic syringe having a diameter of 7 cm, where the syringe head was removed, and the open end was sealed with nylon filter paper tightly. The solution was slowly pushed outside the syringe using the piston until the chitosan solution stops coming outside. The syringe was left with the solid cylinder consisting of mostly PMS and chitosan solution to fill PMS interspacing and hold PMS together. The obtained PMS-chitosan sponge has been kept under a vacuum oven for 48 h at 37 °C to dry it. After the PMS-chitosan sponge dried, (step 2) it was immersed in the PCL 10% (w/v) solution in 1–4 dioxane. The 1–4 dioxane selection was based on the solubility of PCL, but it does not affect PMS and chitosan. The above PCL solution and PMS-chitosan sponge was kept reserved at 700 mmHg of vacuum for 48 h at 37 °C to allow the PCL chains to penetrate the interspacing of sponge created by the dried chitosan. The scaffold was then removed from the PCL solution and followed by the washing with 1–4 dioxane to remove PCL chains stuck on the outer surface of the scaffold. The scaffolds were again dried at similar conditions. In the final step (step 3), the scaffold was immersed in 50 mL of hexane and placed on a rotator shaker at 50 rpm at 37 °C for 48 h, and hexane was kept changing at an interval of 4 h to maintain the kinetics of the solubility of PMS from the scaffold. The scaffold was then dried under similar conditions and stored at 27 °C for the further use. The pure scaffolds, i.e., chitosan and PCL was fabricated, by coating the PMS with respective polymeric solution and leaching it after drying of scaffolds.

Blend fabrication

Both types of scaffolds were fabricated using a similar weight ratio of PCL and chitosan. Briefly, 10% (w/v) PCL and 3% (w/v) chitosan were dissolved in glacial acetic acid separately, and later both the solution was mixed in equal volume ratios and stirred at 37 °C for 3 h. Further, the solution was stored at 4 °C for the fabrication of blend scaffolds (Chi-PCL). The exact process was opted for the fabrication of the Chi-PCL scaffold. However, in the place of chitosan used in step 1 in Sect. 2.2.2, we used a blend of PCL-chitosan and eliminating the step 2 of PCL coating to skip straight to step 3 for the leaching process. The schematic illustration of scaffolds preparation is shown in Fig. 1.

Characterization.

Morphological analysis The scaffolds were analyzed with a scanning electron microscope (Zeiss EVO 40) and a laser scanning confocal microscope (LSM 880, Carl Zeiss). In scaffold analysis, thin slices from each scaffold cross section were taken by cutting them after dipping into the liquid nitrogen. Samples were sputter-coated with gold for 120 s and examined at the 10 kV for SEM analysis. The LSM was performed at 10× using multiple lasers, the rhodamine B (red dye) chitosan, and PCL with malachite green (blue dye). The SEM analysis was performed to observe the surface morphology, nature of the surface coating, pore shape, and size of the scaffolds. LSM was used to identify the presence of both the polymers using the optical method.

Physicochemical analysis X-ray diffraction (XRD) and Fourier-transform infrared spectroscopy (FTIR) were performed to determine the different spectra of C-PCL and Chi-PCL and establish the supposed type of diverse interaction of PCL-chitosan under apart conditions. XRD results also played a role in determining the % crystallinity (% X_c) of the scaffolds. The scaffold XRD patterns were attained using a Bruker, D8 Discover diffractometer (CuK_α radiation) instrument, operated within the 2θ range of 5°–60° by an angle step of 1° min and at 30 kV and 15 mA. The FTIR spectra were recorded in transmittance mode using Spectrum RXI spectrometer in the range of 4000–400 cm^{-1} with a resolution of 1 cm^{-1}.

Mechanical and porosity measurements The amount of load that scaffolds can bear was tested using the cylindrical scaffold sample (7×10 mm), pre-conditioned at 27 °C before testing. The test was performed using UTM Instron-5967 at a set load of 5 kg and mechanical deformation of up to 80% at a speed of 0.5 mm min^{-1}. Archimedes principle was used to measure porosity, in which scaffolds were immersed in a known volume of ethanol (V_1), and the raised volume was noted as (V_2). Afterward, the samples were removed; the left volume of ethanol was marked (V_3). The below-given Eq. (1) was used to calculate the porosity of the samples. The experiments were done in a set of three samples to avoid error in results due to imperfect sample preparation:

$$\text{Porosity}(\%) = \left(\frac{V_1 - V_3}{V_2 - V_1}\right) \times 100. \quad (1)$$

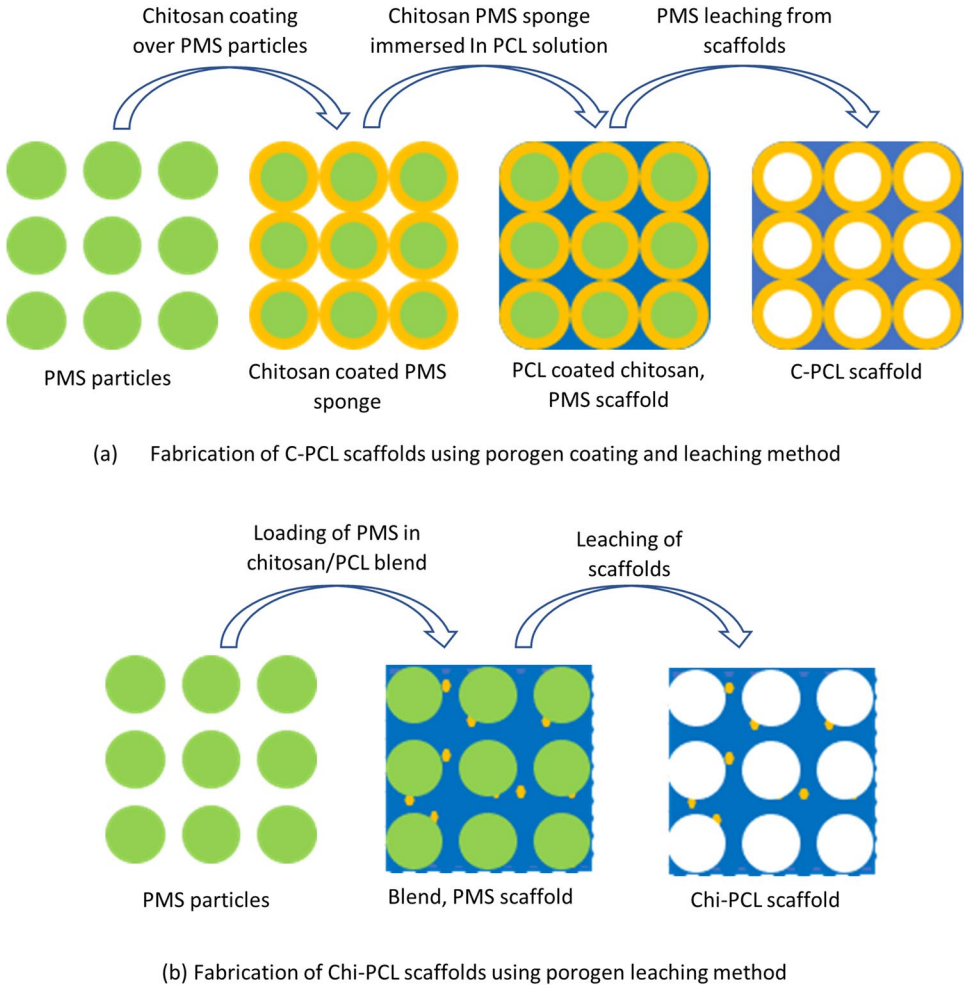

Fig. 1 Schematic illustration for the fabrication of **a** C-PCL and **b** Chi-PCL scaffolds

Thermal analysis Thermal analysis was performed to estimate the thermal stability and thermal transition points and helped us to evaluate the purity and interaction of the scaffolds. Thermogravimetric analysis (TGA) was carried out using a Perkin Elmer instrument at a heating rate of 10 °C min^{-1} in a temperature range of 25–700 °C under a constant nitrogen flow rate of 50 mL min^{-1}. Differential scanning calorimetry (DSC) analysis was carried out using the Mettler Toledo DSC 1 instrument. The sample was first heated till 150 °C for the removal of thermal history, and in the second cycle, the analysis was done in a temperature range of 25–350 °C at 10 °C min^{-1} under the flow of nitrogen gas at the rate of 80 mL min^{-1}. The degree of crystallinity was calculated by Eq. (2), considering ΔH_m^o 139.5 J g^{-1} for 100% crystalline PCL (Pires et al. 2018):

$$\%X_c = \left(\frac{\Delta H_m}{\Delta H_m^o}\right) \times 100. \quad (2)$$

Protein swelling and adsorption study The analysis has been performed to relate the adsorption and swelling ability of the scaffolds with the surface chemistry. Scaffolds (7 × 10 mm) were washed with PBS before the experiment, and then the scaffolds were soaked in PBS solution containing bovine serum albumin (BSA) (1 mg mL^{-1}). The scaffolds were kept at 37 °C for 24 h followed by centrifugation (4000 rpm) for 5 min to extract non-attached BSA molecules. For UV visible analysis, 100 µL of supernatant was mixed with 500 mL of Bradford reagent. It was diluted it with 1 mL of DI followed by monitoring the absorbance at 595 nm to measure the protein mass in unabsorbed media. Swelling behavior was examined under similar conditions by immersing the scaffolds in PBS for 24 h. The wet scaffolds were extracted from the solution and wiped with filter paper to remove excess liquid. The calculation of swelling percentage was done based on Eq. (3), where W_w and $W_d$are the wet and dry weights of scaffolds. The analysis was performed in a triplet to eliminate any error in results.

$$\text{Percentageswelling} = \%S_w = \left(\frac{W_w - W_d}{W_d}\right) \times 100. \quad (3)$$

Biocompatibility analysis of as-synthesized scaffolds

a. *Sterilization of scaffolds* Briefly, the scaffolds (7 × 10 mm) were sterilized using ethylene oxide followed by UV treatment for 30 min on each side. The sterile scaffolds were immersed in a complete medium (DMEM-Low glucose with 10% FBS) for 24 h at 37 °C, 5% CO_2 in a desired well plate.

b. *Cell attachment and morphology assessment* For observing cell attachment, cryopreserved human bone marrow-mesenchymal stem cells (hBM-MSCs) were used [IC-SCR/79/18(o)]. hBM-MSCs were revived and characterized as per the standardized lab protocol (Nandy et al. 2014). Prior to cell seeding, scaffolds were soaked in DMEM low glucose media for 24 h. Onto the as-synthesized scaffolds, 25,000 hBM-MSCs were seeded and were cultured for 48 h in the 37 °C incubators with 5% CO_2. DMEM-Low glucose media with 10% FBS was used for the culture. After 48 h incubation, scaffolds were taken out from the medium and were washed with PBS, followed by fixation using 2.5% glutaraldehyde. Fixed samples were coated with gold for 120 s and then observed under SEM to evaluate cell attachment and morphology.

c. *Cell cytotoxicity assay* Briefly, 10,000 BM-MSCs were seeded onto scaffolds in 48 healthy culture plates and were incubated at 37 °C with 5% CO_2 for 24 h for cell attachment. After 24 h incubation, 10% MTS solution was added to every well, and the well plate was incubated at 37 °C for 3 h. Afterward, media containing MTS solution was collected in another well plate and was read at 490 nm in an ELISA plate reader. After MTS removal, all scaffolds were washed with PBS, and then LG-DMEM media with 10% FBS was added in each well, and the well plate was incubated at 37 °C with 5% CO_2. The experiment was performed thrice in triplicates

d. *Hemocompatibility analysis* For the hemocompatibility study, a fresh blood sample was taken from a healthy rat. Heparin-coated tubes were used for blood collection, and collected blood was centrifuged at 3000 rpm for 10 min for RBC separation. The RBC pellet was diluted with normal saline in a 4:5 ratio for the estimation of hemolysis percentage. The as-synthesized scaffold was incubated with 500 µL of prepared sample and was incubated at 37 °C for 2 h. Normal saline and 1% Triton X-100 were taken as negative and positive controls, respectively. After incubation, RBC: normal saline suspension was taken from each well and centrifuged at 3000 rpm for 10 min. All the experiments were performed in triplicates, and the final absorbance was measured at 540 nm, which indicates the total hemoglobin content in blood plasma. Furthermore, the hemolysis percentage was calculated by following the given Eq. (4).The experiment was performed thrice in triplicates:

$$\text{Hemolysis}\% = \frac{(\text{Abs}_{\text{sample}} - \text{Abs}_{(-)\text{Control}})}{(\text{Abs}_{(+)\text{Control}} - \text{Abs}_{(-)\text{Control}})}. \quad (4)$$

e. *Osteogenic differentiation of hBM-MSCs* Prior to cell seeding, scaffolds were soaked in DMEM-LG with 10% FBS media for 24 h. The next day, media from each well was removed, and all the scaffolds were dried inside the laminar hood. When the scaffolds were dry, 7.5×10^4 hBM-MSCs were re-suspended in 10 µL media and then were seeded onto the scaffolds in 24 well plates. After cell seeding, the well plate was kept in a CO_2 incubator for 2 h for cell attachment. After incubation, DMEM-LG media were added for cell proliferation. Once the cells were 70–80% confluent, DMEM-LG media were replaced with osteocyte induction medium containing low glucose DMEM with 10% FBS, 10 nM dexamethasone, 10 nM β-glycerol phosphate, and 50 µg mL^{-1} ascorbic acid 2 phosphate (Jain et al. 2015). The osteocyte induction medium was changed every 2 days. The culture was continued for 14 days. The experiment was performed thrice in triplicates

f. *Analysis of osteogenic markers* After 14 days of incubation, culture was terminated, and cell-laden composites were dipped in TriReagent for 8–10 h for RNA isolation, and its concentration and purity were analyzed using Nanophotometer, and cDNA was synthesized using SYBR green master mix. GAPDH was used as a house keeping gene, and the osteogenic marker collagen type I (Col-I), alkaline phosphatase (ALP), bone morphogenetic protein 4 (BMP-4), osteocalcin (OCN), and RUNX2 were used to assess the differentiation are summarized in Table S1 (Midha et al. 2021). Data were normalized to un-induced cell-laden composite cultures. RT-PCR was performed for three individual samples ($n = 3$), and all reactions were carried out in multiplicate.

Results and discussion

Characterization of structure and morphology.

The morphology and the structure of the scaffold play a vital role in mechanical strength, adhesion, and cell proliferation. The fundamental concept of the study is to compare Chi-PCL with the scaffold in which bioactivators are coated on the surface of the scaffold pore wall, which may provide the

support and hydrophilic site for the cell to adhere, distribute and proliferate on the homogeneous and interconnected pores network of scaffolds (Maharjan et al. 2021; Vaidhyanathan et al. 2021). The SEM micrograph (Fig. 2) shows the homogeneous and interconnected pore in all the four types of scaffolds, i.e., pure PCL, chitosan, Chi-PCL, and C-PCL. The chitosan is located in the interstitial spacing of the PMS. At the same time, the formation of PMS-chitosan sponge has taken the shape of a pore wall, and with the addition of PCL into the system, the thickness of the pore wall seems to be more regular and thickened (Li et al. 2010). The interconnectivity of the pore has been drawn from the spot where two or more PMS spheres were joined together. Due to which the scaffolds resulted in being highly porous with the interconnected network. The pore size range differed from 100 to 200 µm, consistent with PMS size as a porogen. The achieved pore size and interconnectivity may be adequate for passage of cell, nutrition, and cell growth due to easy cell penetration into the scaffolds (Murphy and O'Brien 2010)**.**

Figure 3 shows the pore wall surface of all the scaffolds (magnified image of Fig. 2) in which PCL seemed to be having a folded and rugged surface with no signs of deposition of any substance over it. Similar results have been observed in the chitosan scaffold case, where the surfaces as slightly rough and consist of few cracks without any deposition. In the Chi-PCL scaffold, the scaffold surface appears to be agglomerated, which may be attributed to the non-compatibility of PCL and chitosan in solution blending (Ghosal et al. 2017). After forming a blend, due to both the polymer immiscible nature, chitosan tends to make a distinct phase, which may be responsible for the twisted surface (Gu et al. 2013). In the case of C-PCL scaffold, the scaffold surface is like PCL scaffolds, but in addition to that, few particle depositions were observed on the surface of the pore wall which may be due to the presence of low quantity of the chitosan available as large quantity may result in film formation over the PCL scaffolds. The above hypothesis was justified using LSM analysis.

In the case of of C-PCL scaffold, the scaffold surface is similar like PCL surface, but in addition to that, few particles depositions were observed on the surface of the pore wall which may be due to low quantity of chitosan available as large quantity may result in the film formation over the PCL scaffolds. To further validate this observation, LSM analysis was performed for the scaffolds. For this, chitosan was marked with red dye. Chitosan was marked with red dye. Blue dye was incorporated in the PCL solution, followed by

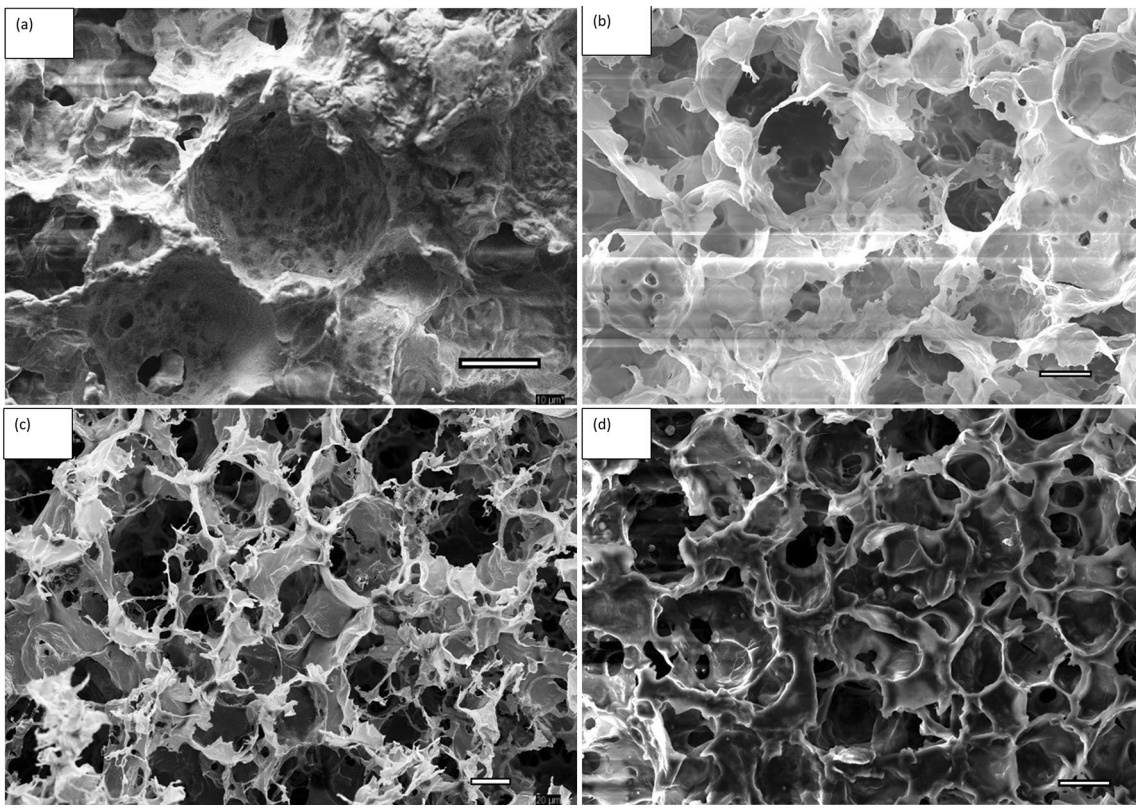

Fig. 2 SEM image of scaffolds **a** PCL, **b** chitosan, **c** Chi-PCL and **d** C-PCL to analyzed the interconnectivity and regularity of the pore and its diameters. Scale 50 µm

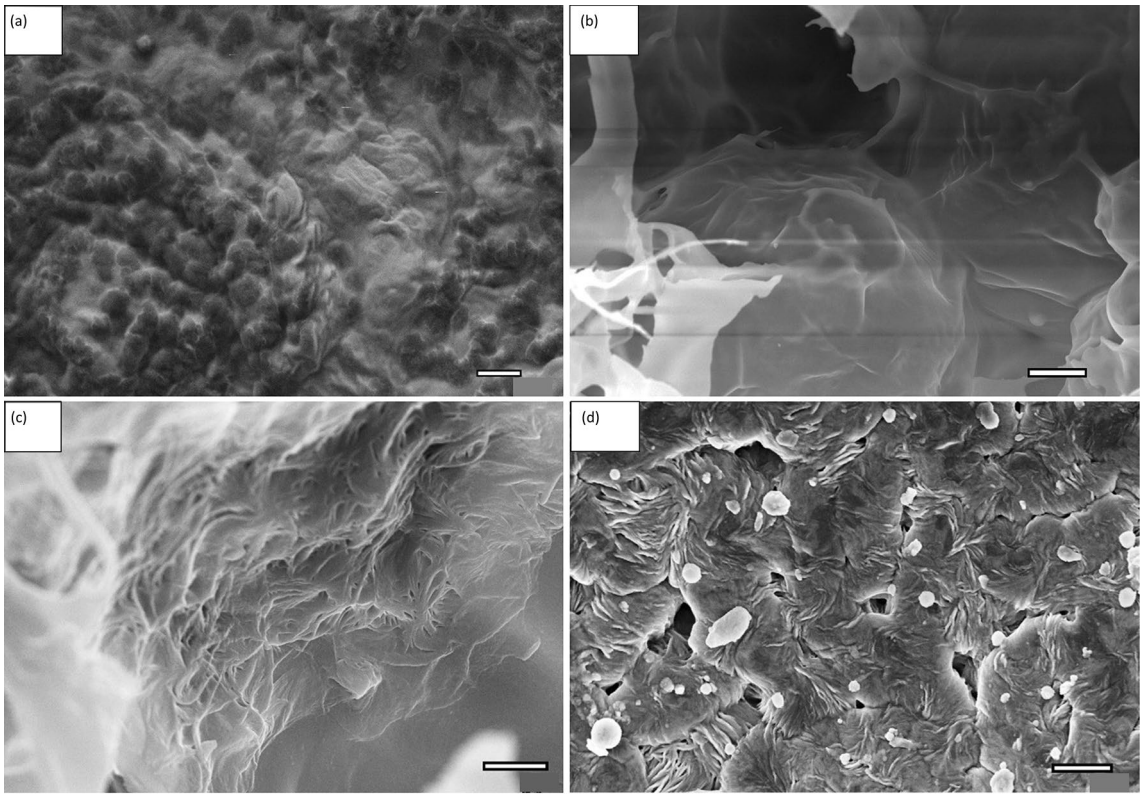

Fig. 3 SEM micrograph at high resolution for the investigation of pore wall surface of the scaffolds **a** PCL, **b** chitosan, **c** Chi-PCL and **d** C-PCL. Scale 5 µm

the scaffold's fabrication. The differential interference contrast (DIC) and colored images of the scaffolds were shown in Fig. 4. The presence of both dyes in distinct places can be seen, which indicated a small amount of chitosan deposition over the PCL layer, marked by a circle. From the image, it can be easily seen that the presence of chitosan is very little in the form of particles lying over the surface of PCL, and the same has been confirmed by the EDX data in (Figure S1 and S2).

Thermal analysis

Thermal gravimetric analysis (TGA)

Figure S3 shows thermal degradation of all the samples and derivative thermo-gravimetric (DTG) analysis. PCL shows 99.62% degradation in the temperature range of 243.2–488.2 °C comprised of two-stage degradation at 300 °C and 404 °C, due to ester pyrolysis and unzipping depolymerization reaction of PCL, respectively (Perumal et al. 2020). Chitosan showed the mass loss in three stages, first at 49.4–110 °C caused by the removal of water bonds, the second peak ($T_{max\ 2}$) appeared at 236 °C for the removal of an amine group from the chitosan molecules, and the final ($T_{max\ 3}$) 318 °C due to primary chain degradation (Habiba et al. 2018). However, Chi-PCL and C-PCL show two stages of mass loss. In Chi-PCL, T_{max} appeared at 348 °C, as compared with chitosan Ch-PCL showing the shifted T_{max} toward the higher values. Chi-PCL blend was thermally more stable than chitosan but at the same time, T_{max} of PCL has been compromised from 404 to 348 °C as Chi-PCL was less stable than PCL (Gautam et al. 2014). The lowering in T_{max} may be responsible for intermolecular interaction between the carbonyl group of PCL and polar groups of chitosan (Martino et al. 2011). In the case of C-PCL, T_{max} was shifted from 318 to 377 °C. This may be attributed to the presence of primarily native PCL chains. The presence of chitosan was significantly low, only in the form of particles lying over its surface. Due to the physical interaction of both polymers, crystallites of PCL were not impaired resulting in a tiny drop in thermal stability of the PCL, suggesting coating technique leads to better thermal stability over the blending technique.

Differential scanning calorimetry (DSC)

Chitosan thermal degradation temperature achieved before its melting point leads to the absence of any transiting peek inside the scan range and the elimination of chitosan DSC thermogram in results. Figure 5 shows data for the remaining three scaffolds. The melting temperature of pure PCL was found to be 57.7 °C having of $\Delta H_m = 83.59\ J\ g^{-1}$,

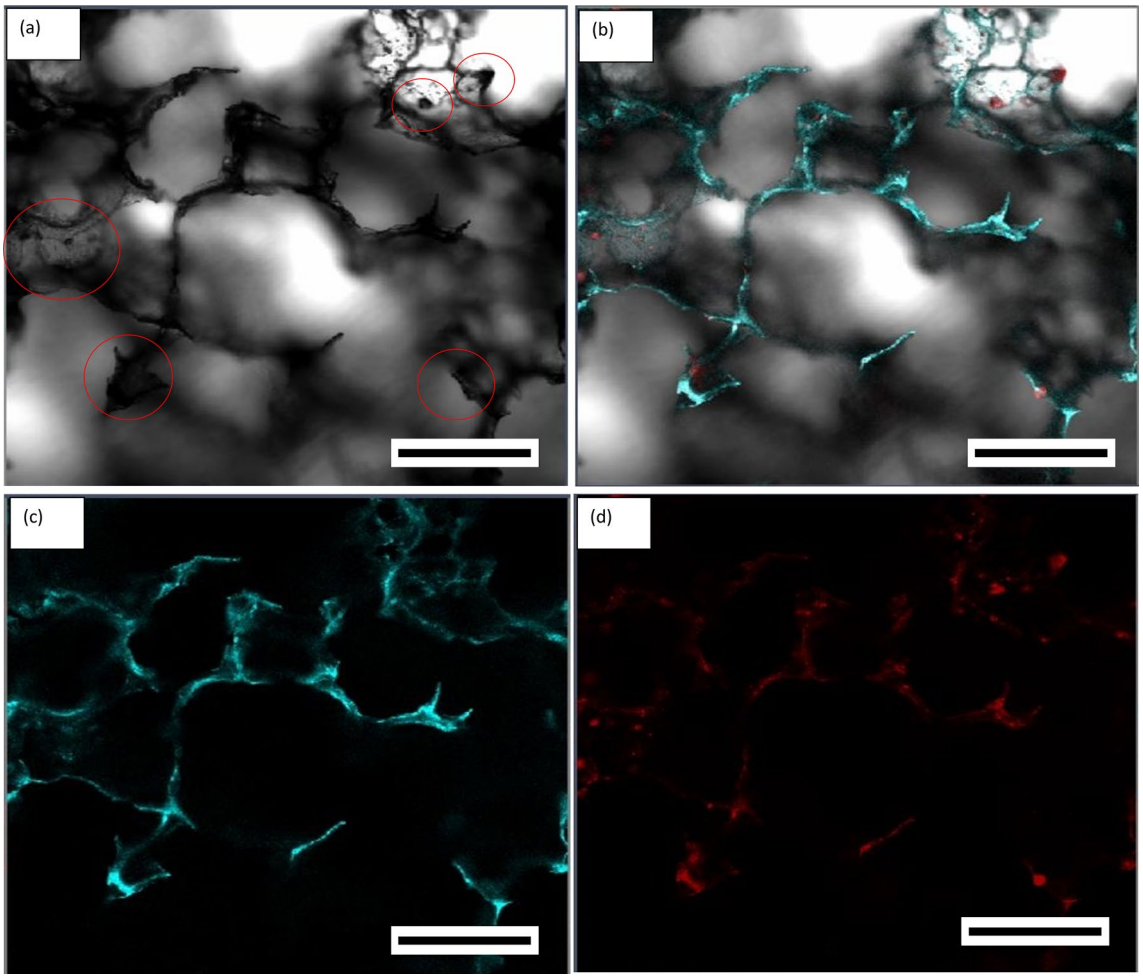

Fig. 4 CLSM image of the C-PCL scaffolds where red dye was incorporated in chitosan and blue dye in PCL. **a** DIC image of C-PCL, **b** combine color image, **c** blue dye (only PCL) and **d** red dye (chitosan). Scale 80 µm

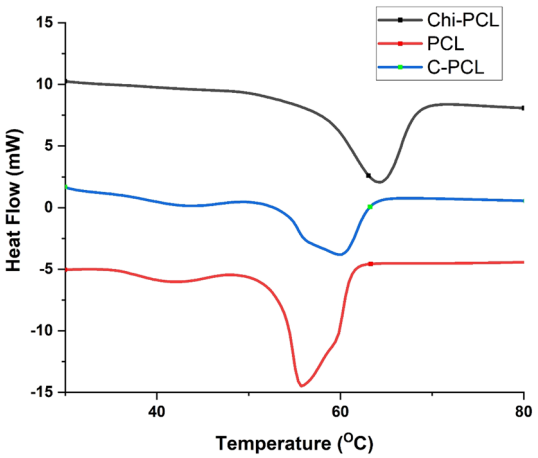

Fig. 5 DSC thermogram of all the different scaffolds

which suggests the $\%X_c$ of the PCL was 59.2%. The scaffolds, C-PCL, and Chi-PCL samples show a slight increase in melting point to 60.0 °C and 64.7 °C, respectively. The increase in the melting point of Chi-PCL may be attributed to chains of chitosan acting as nucleating agents and helping in the PCL chain segmental motion to allow them to achieve better crystallization (Simão et al. 2017). In other cases, the polymer chains interaction was at a lesser degree of extent in Chi-PCL. However, chitosan flacks between the PCL scaffold may act as a reinforcing agent against heat but to a meager extent, though the melting stability was improved by litter considerably compared to pure PCL. The results also reflect the change in $\%X_c$, to 32.99% in Chi-PCL and 29.9% in C-PCL. The crystalline change was attributed to the presence and interaction of chitosan to PCL, and the XRD results have supported the same.

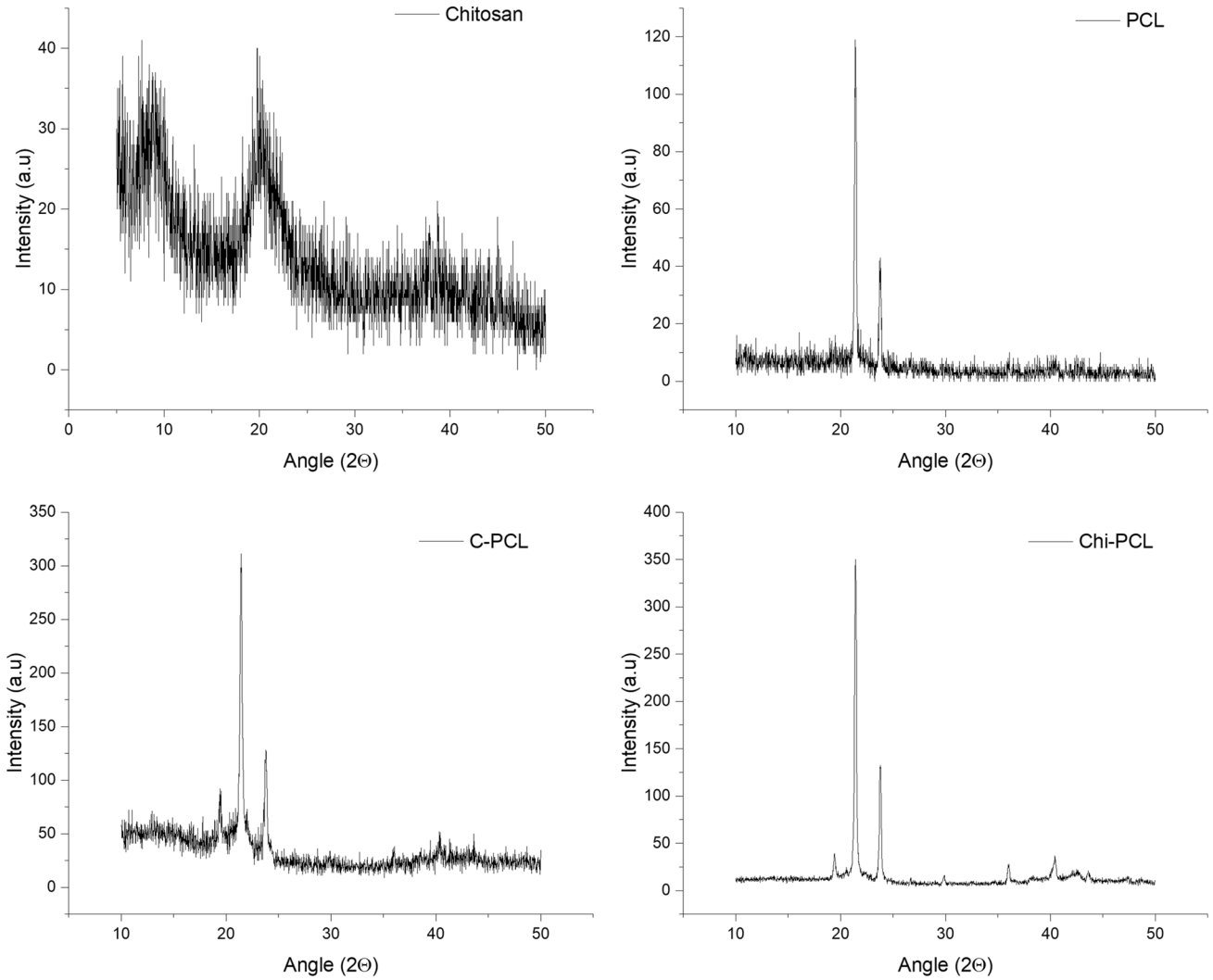

Fig. 6 XRD spectrograph of all the scaffolds used in the study

Physicochemical analysis

X-ray diffraction analysis (XRD)

X-ray diffractogram shown in Fig. 6 in which PCL was estimated sharp peak around 21.38° and 23.7° and broad chitosan peak was appeared at around 8.9° and 20.4°. In contrast, PCL peaks represent (1 1 0) and (2 0 0) planes of polyethylene-like structure, respectively (Abdelrazek et al. 2016). The Chi-PCL and C-PCL show PCL characteristics peak at similar angles. The small chitosan peak was visible at 19.2° due to its low concentration (Sarasam et al. 2006), which confirms the presence of chitosan in both the scaffolds. Nevertheless, in both cases, an increase in crystallinity has been observed. The $\%X_c$ of C-PCL was enhanced compared to Chi-PCL due to the presence of chitosan in PCL scaffolds, which may act as a nucleating agent to improve the PCL chains to arrange them in a close and comparative manner to achieve higher crystallinity.

FTIR spectroscopy

Figure 7 shows the FTIR-spectrogram of both pure polymers along with blend and coated samples. For the Chi-PCL and C-PCL samples, the spectrograph clearly showed all the characteristics peak of chitosan and PCL, indicating the presence of both polymers in the samples. C-PCL shows the absence of any shifting or introduction of new peaks, suggesting no covalent bond formation in the scaffolds. However, physical entanglement may be anticipated. Although in Chi-PCL, all the characteristics peaks were identified, few peaks were shifted toward different wavenumbers. The IR spectrum of Chi-PCL shows peaks at 1754 cm^{-1} and 1215 cm^{-1} instead of the corresponding peak of PCL 1735 cm^{-1} and 1243 cm^{-1}, indicating the shifting of peaks, which may be attributed to some interactions among amino and carbonyl groups of these polymers leading toward the formation of hydrogen bonding.

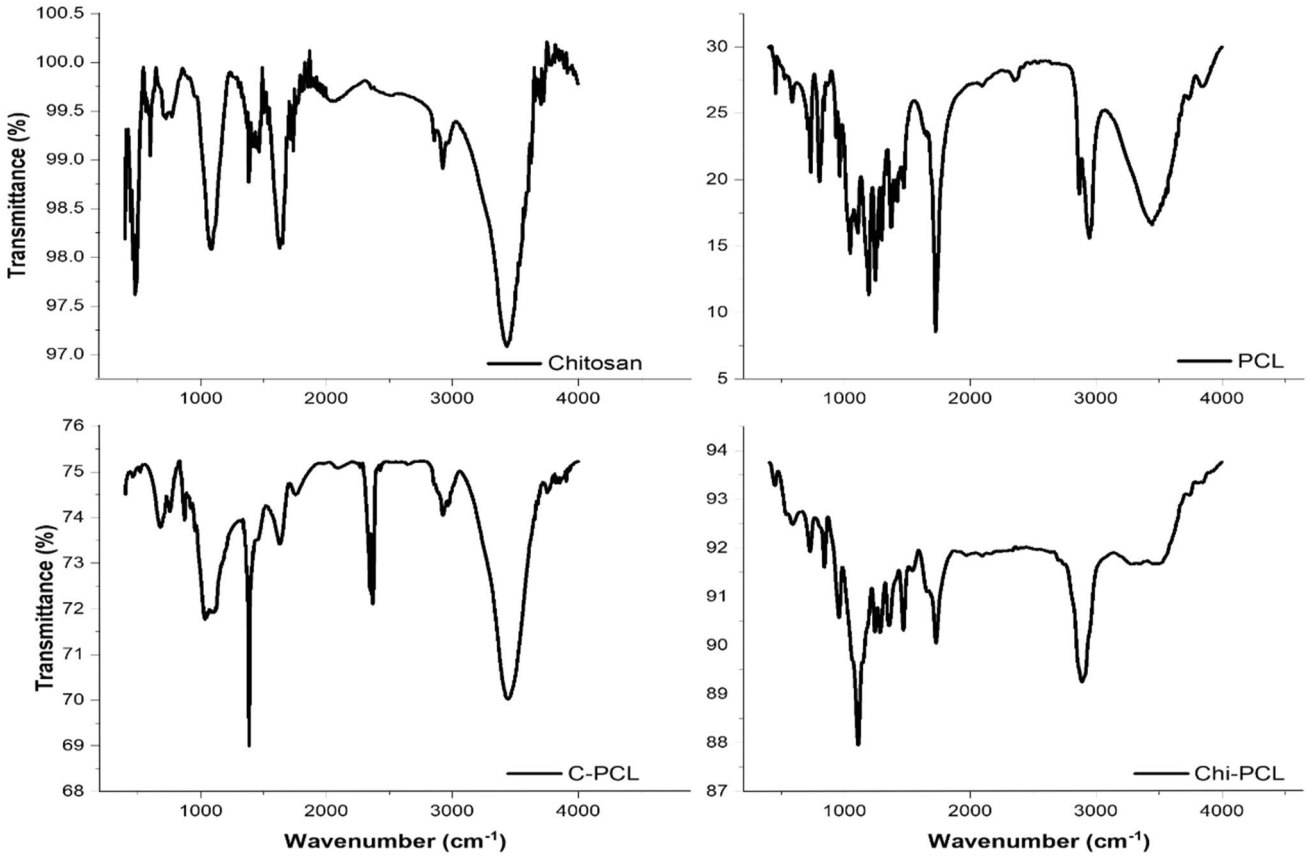

Fig. 7 FTIR spectrograph of all the scaffolds used in the study

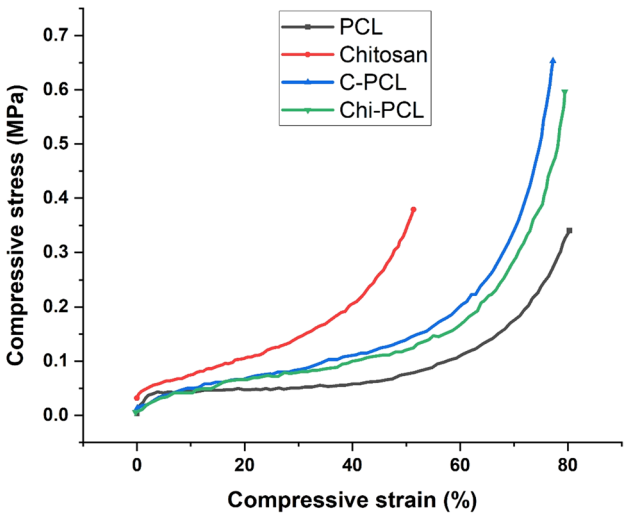

Fig. 8 Stress–strain curve of the scaffolds used in the study for the calculation of mechanical strength of the scaffolds

Mechanical strength

The stress–strain curve of the compression strength is shown in Fig. 8. The stress–strain curve can be divided into three parts for better understanding the nature of scaffolds for different materials. The curve showed three regions, the first elastic region at 5–7% of strain, which shows the scaffolds elastic nature ascribed to skeleton structure of the scaffolds and deform slowly under applied stress. In the second region (at 55–60%), scaffolds deteriorated more linearly than applied stress, resulting in slow deformation of the skeleton of the scaffolds because of the destruction of huge pores present inside them. Still, polymeric scaffolds exhibited the required stiffness to hold the structural integrity for the smooth passage of cells. In the final stage, the porous structure of the scaffolds is crushed and comes closer to form a tight and compacted structure, leading to higher stress for minor deformations. However, due to their structural rigidity, pure PCL and chitosan scaffolds showed the compressive strength of 560 kPa and 400 kPa. Chitosan showed higher and compact packing around the PMS, but due to the porous and brittle nature of the chitosan, it leads to rapid deformation of the porous network and skeleton results in a collapsed

solid bulk, due to which test was performed only by 50% deformation and expected to result in highest compression strength but with lowest structural stability (Madihally and Matthew 1999). Chi-PCL exhibited higher compressive strength (670 kPa) than all the study groups, and C-PCL showed inferior strength (340 kPa) than PCL and Chi-PCL. The enormous decrease in compression strength was explained in terms of chitosan which was initially coated on the PMS surface, leading to the formation of the basic skeleton of the scaffolds. Due to the introduction of PCL, the skeleton might be reinforced to the extent that it can be referred to the structural integrity of the scaffolds. However, due to week skeletons, scaffolds exhibited reduced strength against applied stress. Although C-PCL mechanical strength was lower than PCL and Chi-PCL, at a microscopic level, due to the chitosan coating, scaffolds will easily interact with cells and support the growth and enhance its suitability for the applications.

Porosity measurement

Figure 9 shows the percentage porosity and pore size distribution in all the scaffolds. The porosity and pore size of the PCL, chitosan, and Chi-PCL scaffolds appear to be comparable. It is likely that the removal of PMS has left a slightly smaller size of the void behind it to form the pores. The formation of pores smaller than the used porogen size, may point toward the shrinkage of the scaffolds after removal of the porogen. In samples like PCL and Chi-PCL, due to the higher presence of PCL, the shrinkage phenomenon was less encountered, but the higher content of chitosan leads to the higher shrinkage in the scaffolds (Reyna-Urrutia et al. 2019). Furthermore, the change in the scaffold fabrication technique leads to a slight reduction in porosity 76.04 ± 2.53%.

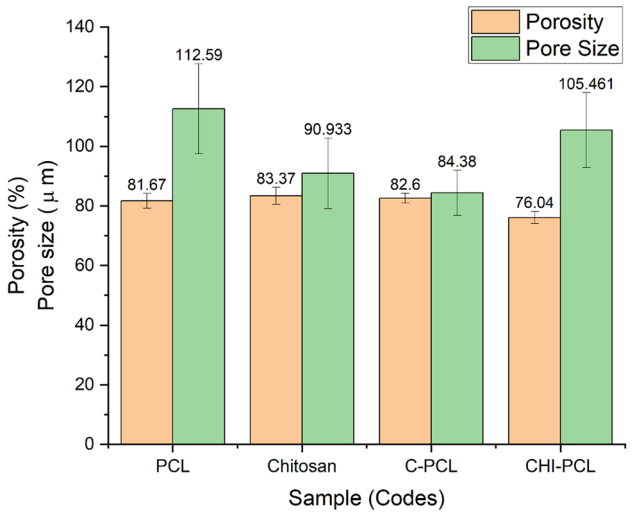

Fig. 9 Calculated porosity percentage and pore size of the all the studied scaffolds

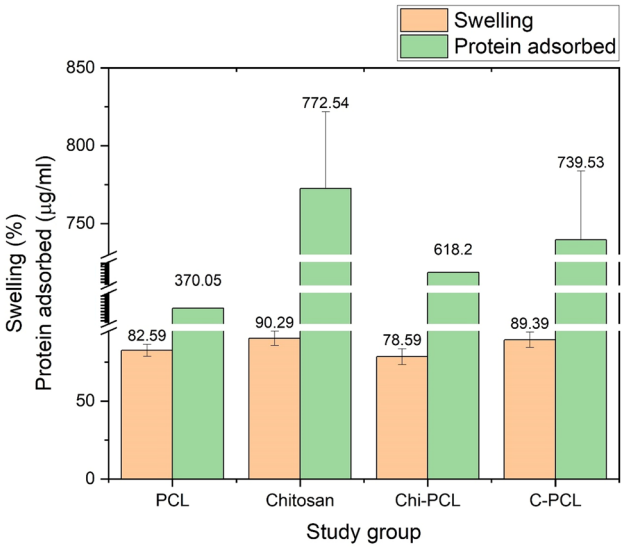

Fig. 10 Percentage swelling and protein adsorption of all the study groups used in study

Protein swelling and adsorption study

The scaffolds exhibited the same behavior in both studies. PCL showed the least, and chitosan showed the most swelling and adsorption in the media, and data are shown in Fig. 10. This can be explained by the presence of functional groups in the polymer molecular structure, as chitosan exhibits hydrophilic groups, such as amine, carboxyl, and hydroxyl groups, which favored the attachment. In contrast, PCL only has an ester group, making this hydrophilic, leading to lower adsorption and swelling behavior (Grigoriadou et al. 2014). However, Chi-PCL showed the protein adsorption of 618 ± 51.73 μg mL^{-1} with a $\%S_w$ of 78.59 ± 5.07%. This may be attributed to the inhomogeneous distribution and exposer of PCL and chitosan layers to the surface of scaffolds. The hydrophobic nature of PCL limited the absorption process. However, C-PCL scaffolds showed more negligible adsorption than chitosan but were superior to any other study groups and can be explained by the presence of chitosan layer on the surface of scaffolds, which supported the absorption process due to the presence of hydrophilic groups, such as ($–NH_2$, –OH, –COOH) (Rodrigues et al. 2020; Esbah Tabaei et al. 2021).

Biological assessment

Cellular viability assay

For evaluation of the toxic potential of scaffolds on BM-MSCs, an MTS assay was performed. Obtained viability

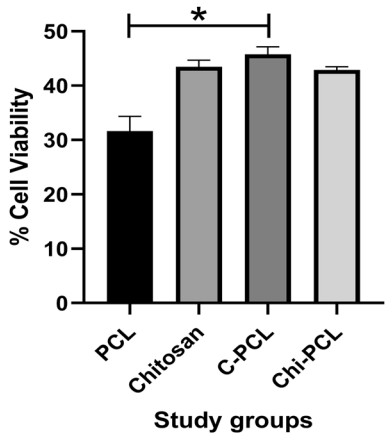

Fig. 11 Cell viability assay for PCL, chitosan, C-PCL and Chi-PCL

percentage is shown in Fig. 11. As per the analysis, the cells seeded on Chi-PCL had similar viability as that of the C-PCL scaffolds, and not much difference was observed between the two in terms of cell viability. The synthesized scaffolds had viability greater than PCL, indicating the poor biocompatibility of the pristine PCL scaffolds, and it could be the result of the hydrophobicity of the PCL (Khorramnezhad et al. 2021). The presence of chitosan has significantly enhanced cell viability by looking at values. It can be seen that the presence of chitosan over the surface has proven to be the best among the study groups (Jiao et al. 2007; Mathews et al. 2008).

Cell attachment and morphology

For cell attachment and morphology analysis, SEM studies were performed. The presence of MSCs was observed on the scaffolds, as depicted in Fig. 12. BM-MSCs formed a confluent sheath of cellular matrix and were observed to be spreading on the C-PCL scaffolds. Proper cell attachment and sheet formation were observed in the Chi-PCL scaffold, but a more spreading and equal distribution of cells was observed on C-PCL. Despite cell attachment on other scaffolds, the presence of chitosan supported the cell adhesion over the surface due to its hydrophilic nature. The presence

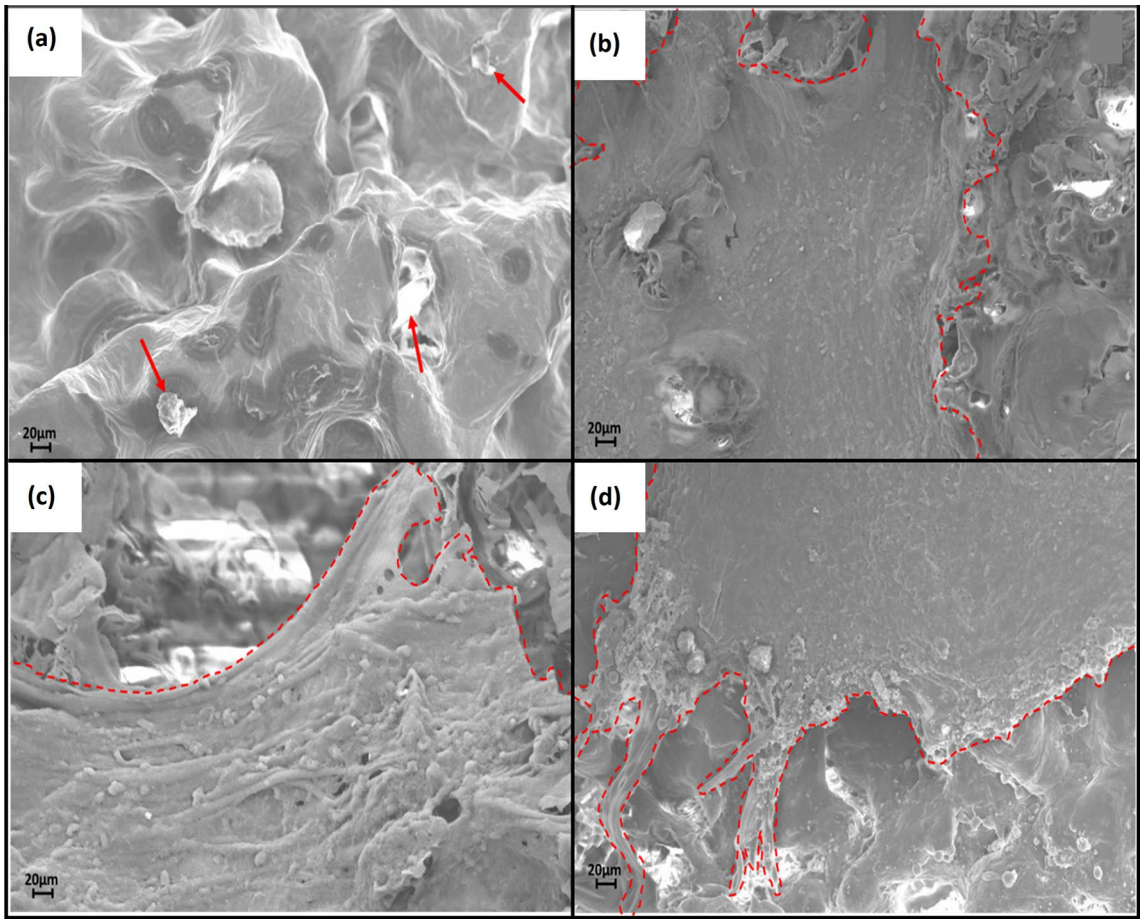

Fig. 12 SEM images for cell attachment and morphology: **a** PCL, **b** chitosan, **c** C-PCL and **d** Chi-PCL. Images were taken at × 500 and scale used is 20 µm

of chitosan may facilitate the binding of protein and cell through multiple cell surface receptors. This may provide a favorable condition for the cell attachment to the pore wall of scaffolds (Duceppe and Tabrizian 2010).

Hemocompatibility assay

For the determination of biocompatibility of the synthesized scaffolds, a hemocompatibility study was performed with RBCs as it is shown in Fig. 13. It was observed that chitosan scaffolds had the highest percentage of hemolysis among all samples, which was around 6%. All other scaffolds were compatible and had a hemolysis percentage lesser than 5% (Shelma and Sharma 2011; Balan and Verestiuc 2014).

Gene expression analysis

Osteocytic differentiation potential of the synthesized scaffolds was quantified through gene expression analysis of major osteogenic makers (Col I, ALP, BMP4, OCN, and RUNX2) (Dutta et al. 2021). Significant markers in bone formation are BMP-4, Col I. Bone mineralization was evaluated using ALP marker expression, and OCN is secreted in osteocytes. For evaluation of early-stage differentiation of MSCs into osteocytes, a Col I marker was used. Col I expression was significantly upregulated in chitosan scaffolds, followed by C-PCL and then Chi-PCL scaffolds. Expression of ALP was prominently high in chitosan, and in fact, chitosan had more expression than the control (TCP). Though lower expression was observed in all other scaffolds, a significant difference between C-PCL and Chi-PCL scaffolds was observed. BMP-4 expression was highest in chitosan, followed by TCP and C-PCL. Like ALP, the remarkable expression of OCN was observed in chitosan scaffolds compared to induced TCP, indicating its supportive osteogenic differentiation. Relatively higher expression of OCN was observed in C-PCL and PCL scaffolds, but the poor expression was observed in the Chi-PCL scaffold. Expression of RUNX2 was highest in induced TCP, followed by chitosan scaffolds. Expression of RUNX2 was very low in all other as-synthesized scaffolds. The results in Fig. 14 indicate that an equal amount of PCL in blend had some derogatory effect because expression of all osteogenic markers was lesser in Chi-PCL than C-PCL.

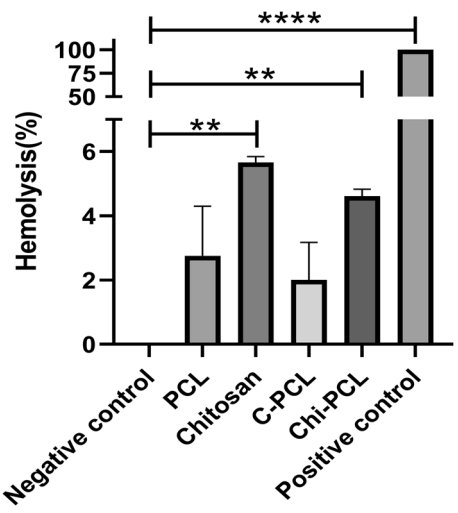

Fig. 13 Hemolysis percentage of as-synthesized scaffolds. Triton X-100 was used a positive control and showed 100% hemolysis was observed. Data are represented in triplicates

Conclusion

The present study compared the two different techniques for the fabrication of three-dimensional porous polymeric scaffolds where the scaffolds were prepared using surface coating methods, using coating of chitosan over the porogen, and transferring the coating to inner pore wall of scaffolds to compare with the conventional method of scaffolds fabrication, i.e., polymer blending. The blending methods lead to masking and limiting the exposure of the bioactive agent on the scaffolds interface, which diminishes the scaffold osteo-conductive properties and cell attachment behavior. The results showed, the surface coating methods overcoming the masking problem of the bioactive agent, and the presence of chitosan over the pore wall surface, which supported the cell growth by providing appropriate conditions for cell growth with similar observation in the cell attachment study. The surface coating of chitosan is clearly shown in SEM and CLSM results. Both fabrication methods have produced excellent cell adhesion and proliferation, attributed to chitosan effectiveness as a carrier of growth factors into the scaffolds.

Furthermore, surface coating methods provided additional advantages, such as scaffolds exhibiting monodispersed (narrow pore size distribution), highly interconnected pores (84.38 ± 7.55 μm) with higher porosity ($82.6 \pm 1.66\%$) and improved protein adsorption 739.53 ± 44.19, as compared to Chi-PCL 618.2 ± 51.73 scaffolds which suggests, the C-PCL had the edge over the Chi-PCL scaffolds due to the ambident cell growth conditions due to the presence of chitosan over the pore wall surface. The notable feature of the C-PCL scaffolds showed a significant difference compared to Chi-PCL when the expression of major osteogenic markers has been analyzed. Expression of all significant markers (Col-I, ALP, BMP-4 OCN, and RUNX-2) of osteocytes was upregulated in C-PCL compared to the Chi-PCL. The results indicated that surface coating methods using porogen coating and leaching techniques showed enhanced and promising results for osteocyte induction. Primary

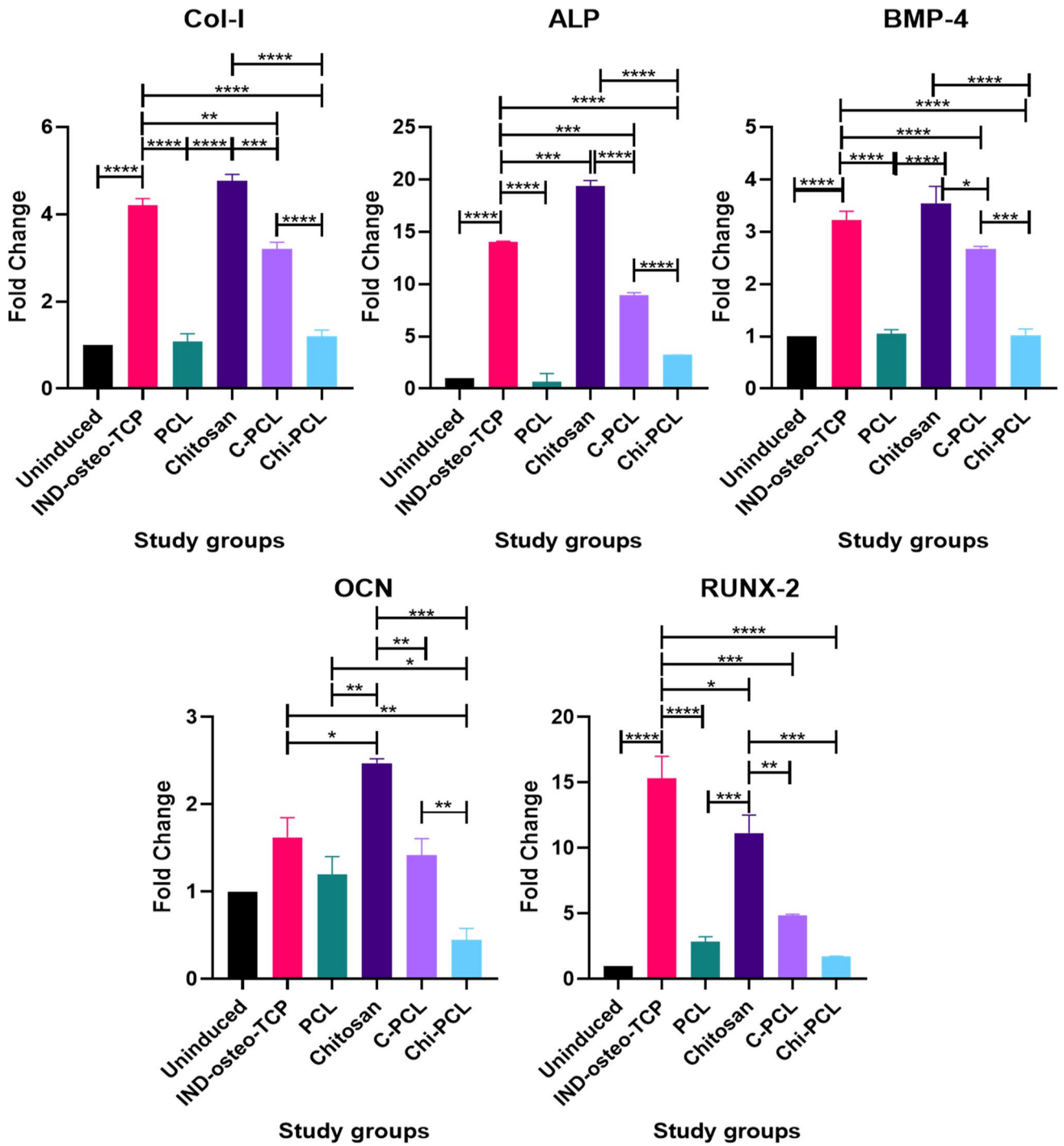

Fig. 14 qRT-PCR assessment of expression of Col-I, ALP, BMP-4, OCN and RUNX-2 for analysis of differentiation of BM-MSCs into osteocytes. Data shown in triplicates and as mean ± SD, ***$p > 0.001$, **$p > 0.05$, *$p > 0.01$

studies based on biomechanical and biocompatibility performance led to the suitability of the material and were verified by further carrying out in vivo and other experiments. However, the limitation of the study is the reduced mechanical strength of the scaffolds. The study can be further extended for in vitro experiments.

Supplementary Information The online version contains supplementary material available at https://doi.org/10.1007/s40204-021-00172-5.

Acknowledgements The author Deepak Poddar gratefully acknowledges Dr. Purnima Jain and Prof. Sujata Mohanty for suggestions and discussion. The author is thankful for the continued support of Stem Cell Facility (DBT-Centre of Excellence for Stem Cell Research)

A.I.I.M.S Delhi for their support and N.S.I.T for providing facility to carry out research work. We acknowledge Prof. Sanjeeve Thakur, Prof. Anjana Sarkar, and Miss Kalpana Pandey for their constant support. The financial support was provided by the Netaji Subhas Institute of Technology, Dwarka, Delhi, India.

Funding This research did not get any specific grant from funding agencies in the public, commercial, or non-profit sectors.

Declarations

Conflict of interest The authors state that this is the original work, and this work or part of work has not been published or considered for publishing elsewhere in any form.

Ethical approval This article does not contain any studies with human participants or animals performed by any of the authors.

References

Abdel-Mohsen M, Richman D, Siliciano RF, Nussenzweig MC, Howell BJ, Martinez-Picado J, Chomont N, Bar KJ, Yu XG, Lichterfeld M, Alcami J, Hazuda D, Bushman F, Siliciano JD, Betts MR, Spivak AM, Planelles V, Hahn BH, Smith DM, Ho YC, Buzon MJ, Gaebler C, Paiardini M, Li Q, Estes JD, Hope TJ, Kostman J, Mounzer K, Caskey M, Fox L, Frank I, Riley JL, Tebas P, Montaner LJ, Abdel-Mohsen M (2020) Recommendations for measuring HIV reservoir size in cure-directed clinical trials. Nat Med 26(9):1339–1350. https://doi.org/10.1038/s41591-020-1022-1

Abdelrazek EM, Hezma AM, El-khodary A, Elzayat AM (2016) Spectroscopic studies and thermal properties of PCL/PMMA biopolymer blend. Egypt J Basic Appl Sci 3(1):10–15. https://doi.org/10.1016/j.ejbas.2015.06.001

Balan V, Verestiuc L (2014) Strategies to improve chitosan hemocompatibility: a review. Eur Polym J 53:171–188

Baptista R, Guedes M (2021) Morphological and mechanical characterization of 3D printed PLA scaffolds with controlled porosity for trabecular bone tissue replacement. Mater Sci Eng C 118:111528. https://doi.org/10.1016/j.msec.2020.111528

Boido M, Ghibaudi M, Gentile P, Favaro E, Fusaro R, Tonda-Turo C (2019) Chitosan-based hydrogel to support the paracrine activity of mesenchymal stem cells in spinal cord injury treatment. Sci Rep 9(1):1–16. https://doi.org/10.1038/s41598-019-42848-w

Chen G, Ushida T, Tateishi T (2000) A biodegradable hybrid sponge nested with collagen microsponges—Chen—2000. J Biomed Mater Res 51(2):273–279. https://doi.org/10.1002/(sici)1097-4636(200008)51:2%3c273::aid-jbm16%3e3.0.co;2-o

Cipitria A, Skelton A, Dargaville TR, Dalton PD, Hutmacher DW (2011) Design, fabrication and characterization of PCL electrospun scaffolds—a review. J Mater Chem 21(26):9419–9453. https://doi.org/10.1039/c0jm04502k

Depan D, Venkata Surya PKC, Girase B, Misra RDK (2011) Organic/inorganic hybrid network structure nanocomposite scaffolds based on grafted chitosan for tissue engineering. Acta Biomater 7(5):2163–2175. https://doi.org/10.1016/j.actbio.2011.01.029

Dhandayuthapani B, Yoshida Y, Maekawa T, Kumar DS (2011) Polymeric scaffolds in tissue engineering application: a review. Int J Polym Sci. https://doi.org/10.1155/2011/290602

Distler T, Fournier N, Grünewald A, Polley C, Seitz H, Detsch R, Boccaccini AR (2020) Polymer-bioactive glass composite filaments for 3D scaffold manufacturing by fused deposition modeling: fabrication and characterization. Front Bioeng Biotechnol 8:552. https://doi.org/10.3389/fbioe.2020.00552

Duceppe N, Tabrizian M (2010) Advances in using chitosan-based nanoparticles for in vitro and in vivo drug and gene delivery. Expert Opin Drug Deliv 7(10):1191–1207. https://doi.org/10.1517/17425247.2010.514604

Dutta SD, Hexiu J, Patel DK, Ganguly K, Lim KT (2021) 3D-printed bioactive and biodegradable hydrogel scaffolds of alginate/gelatin/cellulose nanocrystals for tissue engineering. Int J Biol Macromol 167:644–658. https://doi.org/10.1016/j.ijbiomac.2020.12.011

Esbah Tabaei PS, Asadian M, Ghobeira R, Cools P, Thukkaram M, Derakhshandeh PG, Abednatanzi S, Van Der Voort P, Verbeken K, Vercruysse C, Declercq H, Morent R, De Geyter N (2021) Combinatorial effects of coral addition and plasma treatment on the properties of chitosan/polyethylene oxide nanofibers intended for bone tissue engineering. Carbohydr Polym 253:117211. https://doi.org/10.1016/j.carbpol.2020.117211

Farzinfar E, Paydayesh A (2019) Investigation of polyvinyl alcohol nanocomposite hydrogels containing chitosan nanoparticles as wound dressing. Int J Polym Mater Polym Biomater 68(11):628–638. https://doi.org/10.1080/00914037.2018.1482463

Gao X, Song J, Ji P, Zhang X, Li X, Xu X, Wang M, Zhang S, Deng Y, Deng F, Wei S (2016) Polydopamine-templated hydroxyapatite reinforced polycaprolactone composite nanofibers with enhanced cytocompatibility and osteogenesis for bone tissue engineering. ACS Appl Mater Interfaces 8(5):3499–3515. https://doi.org/10.1021/acsami.5b12413

Gautam S, Chou CF, Dinda AK, Potdar PD, Mishra NC (2014) Fabrication and characterization of PCL/gelatin/chitosan ternary nanofibrous composite scaffold for tissue engineering applications. J Mater Sci 49(3):1076–1089. https://doi.org/10.1007/s10853-013-7785-8

Ghorbani FM, Kaffashi B, Shokrollahi P, Akhlaghi S, Hedenqvist MS (2016) Effect of hydroxyapatite nano-particles on morphology, rheology and thermal behavior of poly(caprolactone)/chitosan blends. Mater Sci Eng C 59:980–989. https://doi.org/10.1016/j.msec.2015.10.076

Ghosal K, Manakhov A, Zajíčková L, Thomas S (2017) Structural and surface compatibility study of modified electrospun poly(ε-caprolactone) (PCL) composites for skin tissue engineering. AAPS PharmSciTech 18(1):72–81. https://doi.org/10.1208/s12249-016-0500-8

Grigoriadou I, Nianias N, Hoppe A, Terzopoulou Z, Bikiaris D, Will J, Hum J, Roether JA, Detsch R, Boccaccini AR (2014) Evaluation of silica-nanotubes and strontium hydroxyapatite nanorods as appropriate nanoadditives for poly(butylene succinate) biodegradable polyester for biomedical applications. Compos Part B Eng 60:49–59. https://doi.org/10.1016/j.compositesb.2013.12.015

Gu C, Gu H, Lang M (2013) Molecular simulation to predict miscibility and phase separation behavior of chitosan/poly(ε-caprolactone) binary blends: a comparison with experiments. Macromol Theory Simul 22(7):377–384. https://doi.org/10.1002/mats.201300109

Habiba U, Siddique TA, Li Lee JJ, Joo TC, Ang BC, Afifi AM (2018) Adsorption study of methyl orange by chitosan/polyvinyl alcohol/zeolite electrospun composite nanofibrous membrane. Carbohydr Polym 191:79–85. https://doi.org/10.1016/j.carbpol.2018.02.081

Jain KG, Mohanty S, Ray AR, Malhotra R, Airan B (2015) Culture & differentiation of mesenchymal stem cell into osteoblast on degradable biomedical composite scaffold: in vitro study. Indian J Med Res 142(6):747–758. https://doi.org/10.4103/0971-5916.174568

Jiao Y, Liu Z, Zhou C (2007) Fabrication and characterization of PLLA-chitosan hybrid scaffolds with improved cell compatibility. J Biomed Mater Res Part A 80(4):820–825. https://doi.org/10.1002/jbm.a.31061

Kane RJ, Roeder RK (2012) Effects of hydroxyapatite reinforcement on the architecture and mechanical properties of freeze-dried

collagen scaffolds. J Mech Behav Biomed Mater 7:41–49. https://doi.org/10.1016/j.jmbbm.2011.09.010
Khorramnezhad M, Akbari B, Akbari M, Kharaziha M (2021) Effect of surface modification on physical and cellular properties of PCL thin film. Colloids Surf B Biointerfaces 200:111582. https://doi.org/10.1016/j.colsurfb.2021.111582
Kim MS, Kim G (2014) Three-dimensional electrospun polycaprolactone (PCL)/alginate hybrid composite scaffolds. Carbohydr Polym 114:213–221. https://doi.org/10.1016/j.carbpol.2014.08.008
Li J, Chen Y, Mak AFT, Tuan RS, Li L, Li Y (2010) A one-step method to fabricate PLLA scaffolds with deposition of bioactive hydroxyapatite and collagen using ice-based microporogens. Acta Biomater 6(6):2013–2019. https://doi.org/10.1016/j.actbio.2009.12.008
Li D, Ye C, Zhu Y, Qi Y, Gou Z, Gao C (2012) Fabrication of poly(lactide-*co*-glycolide) scaffold embedded spatially with hydroxyapatite particles on pore walls for bone tissue engineering. Polym Adv Technol 23(11):1446–1453. https://doi.org/10.1002/pat.2066
Madihally SV, Matthew HWT (1999) Porous chitosan scaffolds for tissue engineering. Biomaterials 20(12):1133–1142. https://doi.org/10.1016/S0142-9612(99)00011-3
Maharjan B, Park J, Kaliannagounder VK, Awasthi GP, Joshi MK, Park CH, Kim CS (2021) Regenerated cellulose nanofiber reinforced chitosan hydrogel scaffolds for bone tissue engineering. Carbohydr Polym 251:117023. https://doi.org/10.1016/j.carbpol.2020.117023
Martino VP, Pollet E, Avérous L (2011) Novative biomaterials based on chitosan and poly(ε-caprolactone): elaboration of porous structures. J Polym Environ 19(4):819–826. https://doi.org/10.1007/s10924-011-0354-9
Mathews DT, Birney YA, Cahill PA, McGuinness GB (2008) Vascular cell viability on polyvinyl alcohol hydrogels modified with water-soluble and -insoluble chitosan. J Biomed Mater Res Part B Appl Biomater 84(2):531–540. https://doi.org/10.1002/jbm.b.30901
Midha S, Jain KG, Bhaskar N, Kaur A, Rawat S, Giri S, Basu B, Mohanty S (2021) Tissue-specific mesenchymal stem cell-dependent osteogenesis in highly porous chitosan-based bone analogs. Stem Cells Transl Med 10(2):303–319. https://doi.org/10.1002/sctm.19-0385
Miszuk J, Liang Z, Hu J, Sanyour H, Hong Z, Fong H, Sun H (2021) Elastic mineralized 3D electrospun PCL nanofibrous scaffold for drug release and bone tissue engineering. ACS Appl Bio Mater 4(4):3639–3648. https://doi.org/10.1021/acsabm.1c00134
Murphy CM, O'Brien FJ (2010) Understanding the effect of mean pore size on cell activity in collagen-glycosaminoglycan scaffolds. Cell Adhes Migr 4(3):377–381. https://doi.org/10.4161/cam.4.3.11747
Naahidi S, Jafari M, Logan M, Wang Y, Yuan Y, Bae H, Dixon B, Chen P (2017) Biocompatibility of hydrogel-based scaffolds for tissue engineering applications. Biotechnol Adv 35(5):530–544. https://doi.org/10.1016/j.biotechadv.2017.05.006
Nahanmoghadam A, Asemani M, Goodarzi V, Ebrahimi-Barough S (2021) Design and fabrication of bone tissue scaffolds based on PCL/PHBV containing hydroxyapatite nanoparticles: dual-leaching technique. J Biomed Mater Res Part A 109(6):981–993. https://doi.org/10.1002/jbm.a.37087
Nair LS, Laurencin CT (2007) Biodegradable polymers as biomaterials. Prog Polym Sci 32(8–9):762–798. https://doi.org/10.1016/j.progpolymsci.2007.05.017
Nandy SB, Mohanty S, Singh M, Behari M, Airan B (2014) Fibroblast growth factor-2 alone as an efficient inducer for differentiation of human bone marrow mesenchymal stem cells into dopaminergic neurons. J Biomed Sci 21(1):1–10. https://doi.org/10.1186/s12929-014-0083-1
Panas-Perez E, Gatt CJ, Dunn MG (2013) Development of a silk and collagen fiber scaffold for anterior cruciate ligament reconstruction. J Mater Sci Mater Med 24(1):257–265. https://doi.org/10.1007/s10856-012-4781-5
Perumal G, Sivakumar PM, Nandkumar AM, Doble M (2020) Synthesis of magnesium phosphate nanoflakes and its PCL composite electrospun nanofiber scaffolds for bone tissue regeneration. Mater Sci Eng C 109:110527. https://doi.org/10.1016/j.msec.2019.110527
Pires LSO, Fernandes MHFV, de Oliveira JMM (2018) Crystallization kinetics of PCL and PCL–glass composites for additive manufacturing. J Therm Anal Calorim 134(3):2115–2125. https://doi.org/10.1007/s10973-018-7307-7
Poddar D, Jain P, Rawat S, Mohanty S (2021) Influence of varying concentrations of chitosan coating on the pore wall of polycaprolactone based porous scaffolds for tissue engineering application. Carbohydr Polym 259:117501. https://doi.org/10.1016/j.carbpol.2020.117501
Raftery RM, Tierney EG, Curtin CM, Cryan SA, O'Brien FJ (2015) Development of a gene-activated scaffold platform for tissue engineering applications using chitosan-pDNA nanoparticles on collagen-based scaffolds. J Control Release 210:84–94. https://doi.org/10.1016/j.jconrel.2015.05.005
Reyna-Urrutia VA, Mata-Haro V, Cauich-Rodriguez JV, Herrera-Kao WA, Cervantes-Uc JM (2019) Effect of two crosslinking methods on the physicochemical and biological properties of the collagen-chitosan scaffolds. Eur Polym J 117:424–433. https://doi.org/10.1016/j.eurpolymj.2019.05.010
Rodrigues C, de Mello JMM, Dalcanton F, Macuvele DLP, Padoin N, Fiori MA, Soares C, Riella HG (2020) Mechanical, thermal and antimicrobial properties of chitosan-based-nanocomposite with potential applications for food packaging. J Polym Environ 28(4):1216–1236. https://doi.org/10.1007/s10924-020-01678-y
Rodrigues ICP, Pereira KD, Woigt LF, Jardini AL, Luchessi AD, Lopes ÉSN, Webster TJ, Gabriel LP (2021) A novel technique to produce tubular scaffolds based on collagen and elastin. Artif Organs 45(5):E113–E122. https://doi.org/10.1111/aor.13857
Saito E, Suarez-Gonzalez D, Murphy WL, Hollister SJ (2015) Biomineral coating increases bone formation by ex vivo BMP-7 gene therapy in rapid prototyped poly(L-lactic acid) (PLLA) and poly(ε-caprolactone) (PCL) porous scaffolds. Adv Healthc Mater 4(4):621–632. https://doi.org/10.1002/adhm.201400424
Sarasam AR, Krishnaswamy RK, Madihally SV (2006) Blending chitosan with polycaprolactone: effects on physicochemical and antibacterial properties. Biomacromol 7(4):1131–1138. https://doi.org/10.1021/bm050935d
Sari M, Hening P, Chotimah AID, Yusuf Y (2021) Porous structure of bioceramics carbonated hydroxyapatite-based honeycomb scaffold for bone tissue engineering. Mater Today Commun 26:102135. https://doi.org/10.1016/j.mtcomm.2021.102135
Saroia J, Yanen W, Wei Q, Zhang K, Lu T, Zhang B (2018) A review on biocompatibility nature of hydrogels with 3D printing techniques, tissue engineering application and its future prospective. Bio-Design Manuf 1(4):265–279. https://doi.org/10.1007/s42242-018-0029-7
Shelma R, Sharma CP (2011) Development of lauroyl sulfated chitosan for enhancing hemocompatibility of chitosan. Colloids Surf B Biointerfaces 84(2):561–570. https://doi.org/10.1016/j.colsurfb.2011.02.018
Shkarina S, Shkarin R, Weinhardt V, Melnik E, Vacun G, Kluger P, Loza K, Epple M, Ivlev SI, Baumbach T, Surmeneva MA, Surmenev RA (2018) 3D biodegradable scaffolds of polycaprolactone with silicate-containing hydroxyapatite microparticles for bone tissue engineering: High-resolution tomography and in vitro study. Sci Rep 8(1):1–13. https://doi.org/10.1038/s41598-018-27097-7
Siddiqui N, Kishori B, Rao S, Anjum M, Hemanth V, Das S, Jabbari E (2021) Electropsun polycaprolactone fibres in bone tissue

engineering: a review. Mol Biotechnol 63(5):363–388. https://doi.org/10.1007/s12033-021-00311-0

Simão JA, Bellani CF, Branciforti MC (2017) Thermal properties and crystallinity of PCL/PBSA/cellulose nanocrystals grafted with PCL chains. J Appl Polym Sci. https://doi.org/10.1002/app.44493

Vaidhyanathan B, Vincent P, Vadivel S, Karuppiah P, Al-Dhabi NA, Sadhasivam DR, Vimalraj S, Saravanan S (2021) Fabrication and investigation of the suitability of chitosan-silver composite scaffolds for bone tissue engineering applications. Process Biochem 100:178–187. https://doi.org/10.1016/j.procbio.2020.10.008

Wei G, Jin Q, Giannobile WV, Ma PX (2006) Nano-fibrous scaffold for controlled delivery of recombinant human PDGF-BB. J Control Release 112(1):103–110. https://doi.org/10.1016/j.jconrel.2006.01.011

Wu H, Lei P, Liu G, Zhang YS, Yang J, Zhang L, Xie J, Niu W, Liu H, Ruan J, Hu Y, Zhang C (2017) Reconstruction of large-scale defects with a novel hybrid scaffold made from poly(L-lactic acid)/nanohydroxyapatite/alendronate-loaded chitosan microsphere: in vitro and in vivo studies. Sci Rep 7(1):1–14. https://doi.org/10.1038/s41598-017-00506-z

Xia T, Liu W, Yang L (2017) A review of gradient stiffness hydrogels used in tissue engineering and regenerative medicine. J Biomed Mater Res Part A 105(6):1799–1812. https://doi.org/10.1002/jbm.a.36034

Xing L, Sun J, Tan H, Yuan G, Li J, Jia Y, Xiong D, Chen G, Lai J, Ling Z, Chen Y, Niu X (2019) Covalently polysaccharide-based alginate/chitosan hydrogel embedded alginate microspheres for BSA encapsulation and soft tissue engineering. Int J Biol Macromol 127:340–348. https://doi.org/10.1016/j.ijbiomac.2019.01.065

Zarrintaj P, Manouchehri S, Ahmadi Z, Saeb MR, Urbanska AM, Kaplan DL, Mozafari M (2018) Agarose-based biomaterials for tissue engineering. Carbohydr Polym 187:66–84. https://doi.org/10.1016/j.carbpol.2018.01.060

Zhao X, Wang H, Fu Z, Li Y (2018) Enhanced interfacial adhesion by reactive carbon nanotubes: new route to high-performance immiscible polymer blend nanocomposites with simultaneously enhanced toughness, tensile strength, and electrical conductivity. ACS Appl Mater Interfaces 10(10):8411–8416. https://doi.org/10.1021/acsami.8b01704